Reversible Dioxygen Binding to Hemerythrin. 1. Electronic Structures of Deoxy- and Oxyhemerythrin

Thomas C. Brunold and Edward I. Solomon*

Contribution from the Department of Chemistry, Stanford University, Stanford, California 94305

Received February 2, 1999

Abstract: Studies on the electronic structure of the two physiologically relevant forms of hemerythrin (Hr), i.e., deoxyHr (possessing a hydroxo-bridged diferrous site) and oxyHr (having an oxo-bridged diferric site with a terminal hydroperoxide), are presented and discussed. SQUID magnetic susceptibility data for deoxyHr confirm that the two ferrous ions are weakly antiferromagnetically coupled, $J = -14(2)$ cm^{-1} ($H = -2J\mathbf{S_1}\cdot\mathbf{S_2}$), indicating that at 300 K the entire manifold of ground-state spin sublevels is available for the reaction with O_2. From density functional calculations on deoxyHr, evaluated on the basis of experimental data, the redox active orbital on the five-coordinate iron (Fe2) is favorably oriented for a π-bonding interaction with O_2 approaching along the open coordination site of that center, and reorientation of the redox active orbital on the six-coordinate iron (Fe1) for electron transfer to O_2 through superexchange with Fe2 is energetically accessible. Analysis of existing spectroscopic data for oxyHr using Heller's time-dependent theory leads to the proposal that the peculiar behavior of the UV resonance Raman excitation profile for the symmetric Fe−O−Fe stretching mode ν(Fe−O) to peak with fairly minor absorption features arises from interference effects between oxo-to-Fe charge-transfer excited states. From density functional calculations on oxyHr and related structures the low frequency of the Fe−oxo stretch is ascribed to the hydrogen bond between the hydroperoxide and the bridging oxide, whereas the small $|J|$ value appears to be due primarily to the strong hydroperoxide → Fe2 π-donor interaction that reduces Fe1 → Fe2 electron delocalization.

1. Introduction

Binuclear non-heme iron active sites occur in a variety of different enzymes and proteins whose functions involve dioxygen binding or activation for further reactions.[1−3] The diversity of the reactions carried out by this class of proteins, such as reversible dioxygen binding to hemerythrin[4] (Hr, dioxygen transport) and O_2 activation by methane monooxygenase[3] (hydroxylation of hydrocarbons), ribonucleotide reductase[5] (generation of a tyrosyl radical), and fatty acid desaturases[6] (reduction of saturated fatty acids), parallels that known for the well-studied heme proteins.[7]

Hemerythrins were the first characterized binuclear non-heme iron proteins.[4,8−11] They constitute one of the three major classes of metalloproteins capable of reversible O_2 binding, which also include the hemoglobins[12] (possessing a heme iron active site) and hemocyanins[13] (having a binuclear Cu active site). The two physiologically relevant forms of Hr are the deoxygenated (deoxyHr) and oxygenated (oxyHr) states[4] (Chart 1). Spectroscopic[9] and crystallographic[14] studies of deoxyHr have shown that the active site consists of two ferrous ions that are bridged by two carboxylates and a water-derived ligand. The coordination spheres of the two irons are completed by five His·N ligands, three binding to the six-coordinate (Fe1) and two to the five-coordinate (Fe2) metal centers (Chart 1).[14] Analyses

Chart 1. Reversible O_2 Binding to Hr

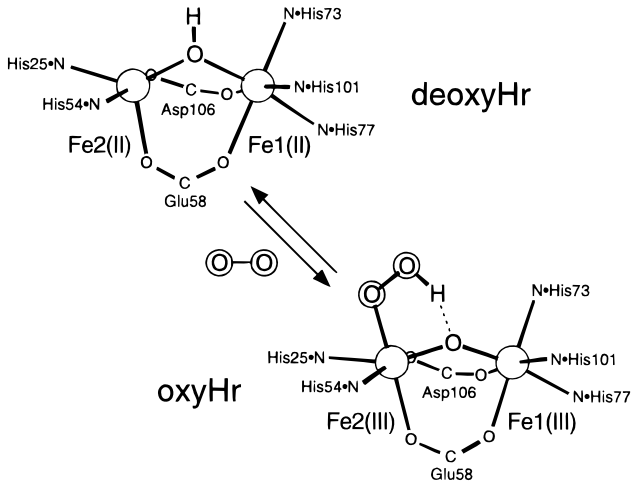

(1) Feig, A. L.; Lippard, S. J. *Chem. Rev.* **1994**, *94*, 759.
(2) Holm, R. H.; Kennepohl, P.; Solomon, E. I. *Chem. Rev.* **1996**, *96*, 2239.
(3) Wallar, B. J.; Lipscomb, J. D. *Chem. Rev.* **1996**, *96*, 2625.
(4) Stenkamp, R. E. *Chem. Rev.* **1994**, *94*, 715.
(5) Logan, D. T.; Su, X.-D.; Åberg, A.; Regnström, K.; Hajdu, J.; Eklund, H.; Nordlund, P. *Struct. Bonding (Berlin)* **1996**, *4*, 1053.
(6) Lindqvist, Y.; Huang, W.; Schneider, G.; Shanklin, J. *EMBO J.* **1996**, *15*, 4081.
(7) Babcock, G. T.; Floris, R.; Nilsson, T.; Pressler, M.; Varortsis, C.; Vollenbrock, E. *Inorg. Chim. Acta* **1996**, *243*, 345.
(8) (a) Wilkins, P. C.; Wilkins, R. G. *Coord. Chem. Rev.* **1987**, *79*, 195. (b) Klotz, I. M.; Kurtz, D. M., Jr. *Acc. Chem. Res.* **1984**, *17*, 16.
(9) (a) Reem, R. C.; Solomon, E. I. *J. Am. Chem. Soc.* **1984**, *106*, 8323. (b) Reem, R. C.; Solomon, E. I. *J. Am. Chem. Soc.* **1987**, *109*, 1216.
(10) Reem, R. C.; McCormick, J. M.; Richardson, D. E.; Devlin, F. J.; Stephens, P. J.; Musselman, R. L.; Solomon, E. I. *J. Am. Chem. Soc.* **1989**, *111*, 4688.
(11) McCormick, J. M.; Reem, R. C.; Solomon, E. I. *J. Am. Chem. Soc.* **1991**, *113*, 9066.
(12) Niederhoffer, E. C.; Timmons, J. H.; Martell, A. E. *Chem. Rev.* **1984**, *84*, 137.
(13) Solomon, E. I.; Baldwin, M. J.; Lowery, M. D. *Chem. Rev.* **1992**, *92*, 521.
(14) Holmes, M. A.; Le Trong, I.; Turley, S.; Sieker, L. C.; Stenkamp, R. E. *J. Mol. Biol.* **1991**, *218*, 583.

10.1021/ja990334s CCC: $18.00
Published on Web 08/31/1999

of variable-temperature magnetic circular dichroism[9] and ^{1}H NMR data[15] revealed that the two ferrous ions of deoxyHr are weakly antiferromagnetically coupled, $-J \approx 12-38$ and $10-20$ cm^{-1}, respectively ($H = -2J\mathbf{S_1}\cdot\mathbf{S_2}$), consistent with a hydroxo bridge at the active site.

In the reaction of deoxyHr with dioxygen one electron from each Fe(II) center and the proton from the bridging hydroxide are transferred to O_2 binding to Fe2, yielding the oxo-bridged diferric site of oxyHr possessing a terminal hydroperoxide (Chart 1).[4] The two-electron reduction of O_2 in oxyHr is confirmed by the appearance of an intense absorption feature at ~500 nm, assigned to a hydroperoxide-to-Fe charge-transfer (CT) transition on the basis of resonance Raman data[16] and polarized single-crystal electronic absorption spectra.[10,17] The presence of an oxo bridge at the active site of oxyHr gives rise to strong antiferromagnetic coupling between the two ferric centers, $J = -77$ cm^{-1}.[18] Compared to other oxo-bridged diferric sites, however, the coupling strength is weaker.[19,20] Also, the vibrational frequency of the symmetric Fe−O−Fe stretching mode ν(Fe−O) is lower in oxyHr than in oxo-bridged diferric model complexes and metHr derivatives.[21] These results were interpreted as indicating a perturbed Fe−oxo bonding interaction in oxyHr, ascribed to the strong hydrogen bond between the hydroperoxide and the bridging oxide (Chart 1) that was identified by Loehr et al.[16,22] using resonance Raman spectroscopy. Yet Mössbauer data[23] do not appear to be consistent with a weakened Fe−oxo interaction: though the quadrupole splitting of one iron is small ($\Delta E_Q \approx 1.0$ mm/s), consistent with a weak Fe−oxo bond, the quadrupole splitting of the second iron ($\Delta E_Q \approx 2.0$ mm/s) is among the largest observed values for Fe(III) in oxo-bridged sites.[24] Another puzzling feature of oxyHr and oxo-bridged ferric dimers in general concerns the UV resonance Raman excitation profile for ν(Fe−O) that tends to peak with fairly minor features in the corresponding CT absorption spectrum.[21]

In this paper, detailed studies on the electronic structure of deoxyHr and oxyHr are reported. SQUID magnetic susceptibility experiments on deoxyHr are presented that permit an accurate determination of the ground-state spin sublevel splitting, an important factor with respect to spin conservation in the reaction of Hr with O_2. Density functional calculations, evaluated on the basis of experimental data, are utilized to explore the nature of the redox active orbitals on the two ferrous centers of the reduced site. For oxyHr, existing spectroscopic data are analyzed in a unified way using Heller's time-dependent theory of electronic absorption and resonance Raman spectroscopy[25] to identify the origin of the unusual spectral features as well as to obtain experimental estimates of the relative donor strengths of the hydroperoxide and the bridging oxide. These results serve as the basis for evaluating and calibrating density functional calculations from which significant insight is obtained into the key geometric features with respect to the electronic structure of oxyHr. The bonding descriptions of deoxyHr and oxyHr generated in this study provide the basis for developing a detailed understanding of the fascinating reaction of O_2 binding to Hr described in the following paper in this issue.

2. Experimental Section

DeoxyHr Magnetization Studies. Hr was isolated from the coelomic fluid of *Phascolopsis gouldii* obtained live from the Marine Biological Laboratory, Woods Hole, MA. After standard purification[26] the protein was dialyzed against 0.2 M Tris(SO_4^{2-}), pH 7.7. Stock solutions of deoxyHr were prepared by dialyzing the protein anaerobically first against ~10 mM $Na_2S_2O_4$ for at least 12 h and subsequently against buffer to remove excess dithionite. The deoxyHr concentration was determined spectrophotometrically after air oxidation to oxyHr (ϵ(500 nm) = 2200 M^{-1} cm^{-1}).[27] Apoprotein was prepared following initial conversion of oxyHr into metHr, as described in ref 28. Magnetic susceptibility data were collected using a SQUID magnetometer (Quantum Design Model MPMS). About 100 μL of ~4 mM protein solution was transferred into a gelatin capsule and immediately frozen in liquid N_2. To eliminate contributions from the protein moiety and the buffer, a sample of apoprotein in 0.2 M Tris(SO_4^{2-}) buffer was measured under identical conditions and subtracted from the deoxyHr data.[29] The susceptibility data were analyzed using the following spin Hamiltonian:[9,30]

$$H = -2J\mathbf{S_1}\cdot\mathbf{S_2} + \sum_{i=1}^{2}\left\{D_i\left(\mathbf{S_{zi}}^2 - \frac{1}{3}S(S+1)\right) + E_i(\mathbf{S_{xi}}^2 - \mathbf{S_{yi}}^2) + \beta\mathbf{H}\cdot\mathbf{g_i}\cdot\mathbf{S_i}\right\} \quad (1)$$

J is the exchange coupling constant, D_i and E_i are the axial and rhombic ZFS parameters and $\mathbf{g}_i$ are the principal g values of the two Fe(II) ions ($i = 1, 2$), and $\mathbf{H}$ represents the magnetic field. The magnetization was calculated using the formalism developed by Vermaas and Groeneveld[31] and fitted to the experimental data to obtain the spin Hamiltonian parameters. To test the sensitivity of the fitted J value to the other parameters, fits were perfomed with D_i and E_i kept constant within reasonable limits, and the principal axes of the $\mathbf{D}$ tensors on the two ferrous ions were rotated relative to each other.

OxyHr Data Treatment. A normal coordinate analysis (NCA) of the vibrational data of oxyHr was performed on the C_s symmetrized HO_2−Fe−O−Fe unit of oxyHr (structural parameters were taken from the geometry-optimized oxyHr model; see below). The analysis was based on a Wilson FG matrix method using a Urey−Bradley force field as implemented in a modified version of the Schachtschneider program.[32]

(15) Maroney, M. J.; Kurtz, D. M., Jr.; Nocek, J. M.; Pearce, L. L.; Que, L., Jr. *J. Am. Chem. Soc.* **1986**, *108*, 6871.
(16) Shiemke, A. K.; Loehr, T. M.; Sanders-Loehr, J. *J. Am. Chem. Soc.* **1984**, *106*, 4951.
(17) Gay, R. R.; Solomon, E. I. *J. Am. Chem. Soc.* **1978**, *100*, 1972.
(18) Dawson, J. W.; Gray, H. B.; Hoenig, H. E.; Rossman, G. R.; Schredder, J. M.; Wang, R. H. *Biochemistry* **1972**, *11*, 461.
(19) Kurtz, D. M., Jr. *Chem. Rev.* **1990**, *90*, 585.
(20) From susceptibility measurements[18] the J values for oxyHr (−77 cm^{-1}) and metHr (−134 cm^{-1}) are substantially different; however, ^{1}H NMR data[15] appear to indicate that this difference is less pronounced.
(21) Sanders-Loehr, J.; Wheeler, W. D.; Shiemke, A. K.; Averill, B. A.; Loehr, T. M. *J. Am. Chem. Soc.* **1989**, *111*, 8084.
(22) Shiemke, A. K.; Loehr, T. M.; Sanders-Loehr, J. *J. Am. Chem. Soc.* **1986**, *108*, 2437.
(23) Clark, P. E.; Webb, J. *Biochemistry* **1981**, *20*, 4628.
(24) Que, L., Jr.; True, A. E. In *Progress in Inorganic Chemistry: Bioinorganic Chemistry*; Lippard, S. J., Ed.; John Wiley & Sons: New York, 1990; pp 97−200.
(25) Tannor, D. J.; Heller, E. J. *J. Chem. Phys.* **1982**, *77*, 202.
(26) Klotz, I. M.; Klotz, T. A.; Fiess, J. A. *Arch. Biochem. Biophys.* **1957**, *68*, 284.
(27) Garbett, K.; Darnall, D. W.; Klotz, I. M.; Williams, R. J. P. *Arch. Biochem. Biophys.* **1969**, *135*, 419.
(28) Zhang, J. H.; Kurtz, D. M., Jr.; Xia, Y.-M.; Debrunner, P. G. *Biochemistry* **1991**, *30*, 583.
(29) While qualitatively very similar results were obtained from different samples, some variations in absolute intensity were observed, reflecting varying amounts of oxyHr and denatured protein in our samples. Because of the large J value for oxyHr, however, the formation of oxidized protein will primarily result in a reduction in magnetization intensity by a constant factor (due to a decrease in deoxyHr concentration), and iron released upon protein denaturation will predominantly perturb the low-temperature susceptibility data. Thus, the presence of oxyHr and denatured protein in our samples of deoxyHr should only weakly affect the qualitative behavior of the χT curves.
(30) Kennedy, B. J.; Murray, K. S. *Inorg. Chem.* **1985**, *24*, 1552.
(31) Vermaas, A.; Groeneveld, W. L. *Chem. Phys. Lett.* **1974**, *27*, 583.
(32) (a) Schachtschneider, J. H. Technical Report No. 57-65, Shell Development Co., Emeryville, CA, 1966. (b) Fuhrer, H.; Kartha, V. B.; Kidd, K. G.; Krueger, P. J.; Mantsch, H. H. Computer Programs for Infrared Spectroscopy, Bulletin No. 15, National Research Council of Canada, 1976.

Table 1. Experimental Band Maxima,[9] ν_{exp}, and Calculated Transition Energies, ν_{calc}, for DeoxyHr (cm^{-1})

	six-coordinate Fe1		five-coordinate Fe2	
ν_{exp}	$yz \rightarrow$	ν_{calc}	$yz \rightarrow$	ν_{calc}
11600	xy	11500		
10350			z^2	10910
8800	z^2	9500		
~5000			$x^2 - y^2$	3820
	xz	1610	xy	2920
	$x^2 - y^2$	390	xz	1550

Simultaneous fits of the absorption and resonance Raman excitation profile data of oxyHr were performed using the time-dependent theory of electronic spectroscopy[25,33] implemented in a script for Mathcad PLUS 6.0. A direct modeling approach as described in ref 34 was used to search for the set of excited-state parameters that produce the best simultaneous fit of the absorption and resonance Raman profile data.

Electronic Structure Calculations. Density functional calculations were performed on IBM 3BT-RS/6000 work stations using the Amsterdam Density Functional (ADF) program version 2.0.1 developed by Baerends et al.[35] A triple-ζ Slater-type orbital basis set (ADF basis set IV) with a single polarization function was used for each atom. Core orbitals were frozen through 1s (N, O) and 3p (Fe). All calculations were performed employing the local density approximation of Vosko, Wilk, and Nusair[36] and the nonlocal gradient corrections of Becke[37] and Perdew.[38] The active site structures of deoxyHr and oxyHr (Chart 1) were approximated by models in which formates replace the carboxylates and NH_3 ligands replace the histidines. The coordinates were taken from the Brookhaven Protein Data Bank (files 1HMD and 1HMO, respectively), averaged for the four molecules in the asymmetric unit,[14] and adjusted to the more accurate EXAFS bond lengths.[4] Because of the large distribution in possible positions of the μ-O(H) bridge and the hydroperoxide, the coordinates of the corresponding atoms were obtained[39] through energy minimization by using the algorithm of Versluis and Ziegler.[40] Complete coordinates of all the models employed for the calculations presented in the text are included in the Supporting Information.

3. Results and Analysis

3.1. Deoxyhemerythrin. Data and Analysis. In previous studies of deoxyHr employing absorption, circular dichroism (CD), and magnetic CD (MCD) spectroscopies,[9] a total of four ligand field (LF) transitions could be identified in the near-IR region (Table 1), consistent with the presence of one six-coordinate (Fe1) and one five-coordinate (Fe2) ferrous ion (Chart 1). From variable-temperature MCD[9] and ^{1}H NMR experiments[15] the two irons are antiferromagnetically coupled, $-J \approx 12-38$ and $10-20$ cm^{-1}, respectively.

To obtain a more direct estimate of J, SQUID magnetization data were taken on deoxyHr (Figure 1).[29] While simulations using the spin Hamiltonian in eq 1 revealed that the experimental data do not permit an accurate determination of the single-site ZFS parameters, the value of J obtained from fits of χT curves is well determined by the susceptibility data. Reasonable fits are obtained with $J = -14(2)$ cm^{-1} (Figure 1, solid line), indicating weak antiferromagnetic coupling between the two ferrous ions and consistent with the hydroxide bridge at the deoxyHr site.[14]

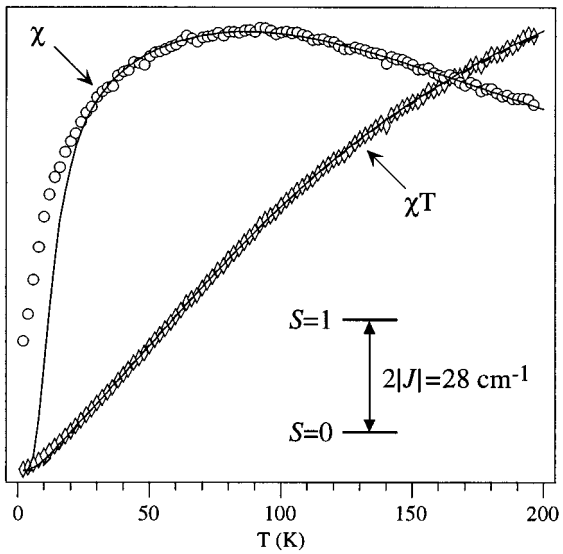

Figure 1. Magnetic susceptibility data for deoxyHr. The solid lines were obtained using the spin Hamiltonian in eq 1 with $J = -14$ cm^{-1}, $g = 2.0$, and $D_i = E_i = 0$ cm^{-1}.

Electronic Stucture Calculations and Comparison to Data. An energy level diagram obtained from a broken symmetry (BS, $M_S = 0$) density functional calculation on deoxyHr is shown in Figure 2, and the energies and compositions of the relevant Fe1 and Fe2 d-based molecular orbitals (MOs) are given in Table 2 (the molecular (primed) and local (unprimed) coordinate frames are defined[41] in Figure 2, top). To validate a more detailed consideration of the calculated MO descriptions, the computational results are first evaluated on the basis of experimental data. (i) Using the formalism developed by Noodleman,[42] the ground-state exchange coupling constant J can be estimated from the energies (E) of the high-spin (HS, $S = S_{max} = 4$) and BS states

$$J = -(E_{HS} - E_{BS})/{S_{max}}^2 \qquad (2)$$

yielding $J = +7$ cm^{-1}. Thus, while the calculation gives the wrong sign of J, it is consistent with the experimental finding of weak exchange coupling ($J = -14$ cm^{-1}). (ii) The energies of the spin-allowed ligand field (LF) transitions of each Fe were calculated from the differences in total energies of the excited states and the ground state at convergence (Table 1). The correspondence with the experimental results is satisfactory: the calculation predicts two transitions for Fe1 and a single transition for Fe2 in the $8000-12000$ cm^{-1} region, as observed.[9,43] Thus, a more detailed analysis of the calculated electronic structure description of deoxyHr is justified.

Bonding Description. Nature of the Fe d-Based Orbitals. From crystallographic studies[14] the ligand environment of the five-coordinate Fe2 was described as distorted trigonal bipyramidal with a pseudo-C_3 axis oriented along the His54·N−Fe2−Asp106·O vector (Chart 1), consistent with the calculated splitting pattern of the LF excited states of that iron (Table 1).[44] In the ground state the extra electron occupies the yz-based spin-

(33) Zink, J. I.; Shin, K. S. K. *Adv. Photochem.* **1991**, *16*, 119.
(34) Myers, A. B.; Mathies, R. A. In *Biological Applications of Raman Spectroscopy*; Spiro, T. G., Ed.; Wiley: New York, 1987; Vol. 2, pp 1−58.
(35) (a) Baerends, E. J.; Ellis, D. E.; Ros, P. *Chem. Phys.* **1973**, *2*, 42. (b) te Velde, G.; Baerends, E. J. *Int. J. Comput. Phys.* **1992**, *99*, 84.
(36) Vosko, S. H.; Wilk, L.; Nusair, M. *Can. J. Phys.* **1980**, *58*, 1200.
(37) Becke, A. D. *J. Chem. Phys.* **1986**, *84*, 4524.
(38) Perdew, J. P. *Phys. Rev. B* **1986**, *33*, 8822.
(39) Selected distances (Å) and angles (deg) for deoxyHr, Fe1−O^H = 2.07, Fe2−O^H = 2.02, Fe1−O−Fe2 = 110, and oxyHr, Fe1−O = 1.85, Fe2−O = 1.88, Fe2−Oa = 2.00, Oa−Ob = 1.41, Fe1−O−Fe2 = 125, Fe2−Oa−Ob = 116.
(40) Versluis, L.; Ziegler, T. *J. Chem. Phys.* **1988**, *88*, 322.
(41) The local coordinate systems on each Fe center are defined by the principal axes of the respective **D** tensors that were calculated as described. Neese, F.; Solomon, E. I. *Inorg. Chem.* **1998**, *37*, 6568.
(42) Noodleman, L. *J. Chem. Phys.* **1981**, *74*, 5737.
(43) The relative energies of the Fe d-based MOs (Figure 2, Table 2) and the corresponding LF excited states (Table 1) differ substantially, indicating that electronic relaxation effects upon excitation are important.

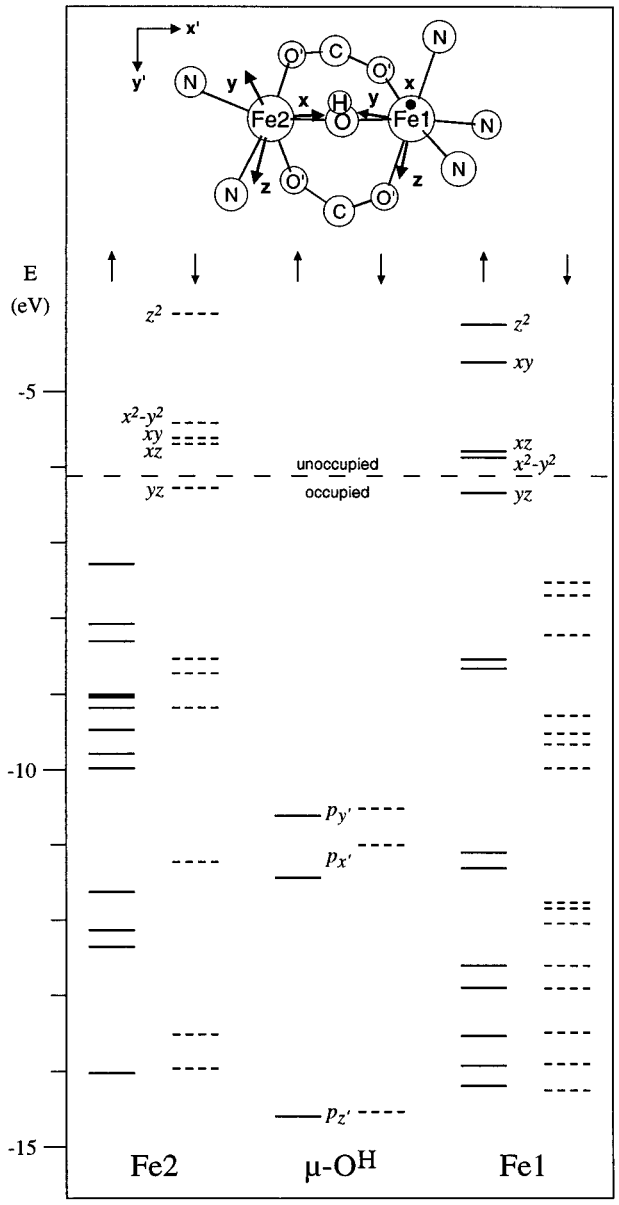

Figure 2. Energy level diagram obtained from a BS ($M_S = 0$) calculation on deoxyHr. Spin-up and spin-down levels are shown by solid and broken lines, respectively. Top portion: deoxyHr model employed, along with the molecular (primed) and local (unprimed) coordinate frames.

down molecular orbital (MO) that is largely stabilized in energy relative to its four unoccupied partners (Figure 2).

The splitting pattern of the quintet LF states of Fe1 (Table 1) is typical of a distorted octahedral ligand environment with a weak axial LF component, consistent with the long His73·N−Fe1−Glu58·O bonds[14] (Chart 1). In the ground state the extra electron of Fe1 occupies the *yz*-based spin-up MO; however, the $yz \rightarrow x^2 - y^2$ LF excited state is only ~390 cm^{-1} higher in energy (Table 1).

Interaction with the Bridging Hydroxide. The low hydroxide (O^H) orbital character in the Fe d-based MOs (Table 2) indicates that the Fe−hydroxide bonding interaction is weak. From Figure 2, the weakness of this interaction can be attributed to the large energy difference between the Fe d- and O^H p-based MOs. The proton of the bridging hydroxide greatly stabilizes

(44) (a) Solomon, E. I.; Pavel, E. G.; Loeb, K. E.; Campochiaro, C. *Coord. Chem. Rev.* **1995**, *144*, 369. (b) Pavel, E. G.; Kitajima, N.; Solomon, E. I. *J. Am. Chem. Soc.* **1998**, *120*, 3949.

Table 2. Relative energies, E_{rel} (eV), and Compositions (%) of the Relevant Fe d-Based MOs Obtained from a BS Calculation on DeoxyHr (Figure 2, top)[a]

Spin-Up Orbitals Localized on Fe1

level	E_{rel}	Fe1	O^H	Fe2	O′	N
		Unoccupied				
z^2	2.223	83	0	0	3	3
xy	1.730	78	2	0	2	3
xz	0.551	92	2	0	1	0
$x^2 - y^2$	0.464	93	1	0	1	0
		Occupied				
yz	0.000	94	0	0	1	0

Spin-down Orbitals Localized on Fe2

level	E_{rel}	Fe2	O^H	Fe1	O′	N
		Unoccupied				
z^2	2.298	66	1	0	4	3
$x^2 - y^2$	0.855	83	1	0	3	1
xy	0.664	87	5	1	2	1
xz	0.584	93	3	0	1	0
		Occupied				
yz	0.000	93	0	0	2	0

[a] Fe d, O^H (μ-hydroxo) p, and total O′ (formate) and N (NH_3) orbital contributions.

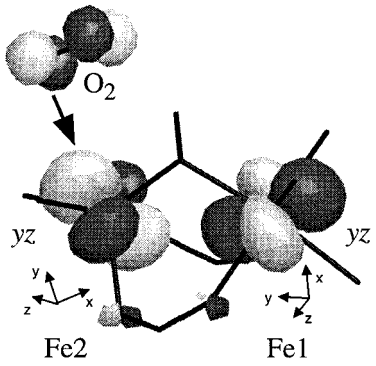

Figure 3. Boundary surface plots of the redox active orbitals containing the extra (spin-up) electron of Fe1 and the extra (spin-down) electron of Fe2, obtained from a BS ($M_S = 0$) calculation on deoxyHr. Also indicated is the favorable orientation of the Fe2-centered orbital for a π-bonding interaction with one of the π^* orbitals of O_2 approaching along the open coordination site of that center.

the O p orbitals, in particular the $p_{z'}$ level as this is involved in a strong σ-bonding interaction with the proton. The bridging hydroxide is therefore a poor mediator of exchange coupling, and the Fe d-based MOs localized on one iron exhibit very little orbital contributions from the other metal, consistent with the small experimental *J* value.

Redox Active Orbitals. Of particular interest with respect to the reactivity of deoxyHr toward O_2 are the orientations of the redox active MOs containing the extra electron on each iron relative to the dimer structure. The *yz*-based spin-down orbital localized on the five-coordinate Fe2 is properly oriented for a π-bonding interaction with one of the two half-occupied π^* orbitals of dioxygen approaching along the open coordination site (Figure 3). The redox active orbital on the six-coordinate Fe1 is oriented perpendicular to the Fe1−O^H bond that might be anticipated to play a key role for electron transfer from Fe1 to O_2 binding to Fe2. The $yz \rightarrow x^2 - y^2$ excited state of that iron is only ~390 cm^{-1} above the ground state (Table 1), however, and the $x^2 - y^2$-based spin-up MO has a good orientation for a π-bonding interaction with O^H. Thus, rehybridization of the Fe1 *yz* and $x^2 - y^2$ orbitals to properly orient

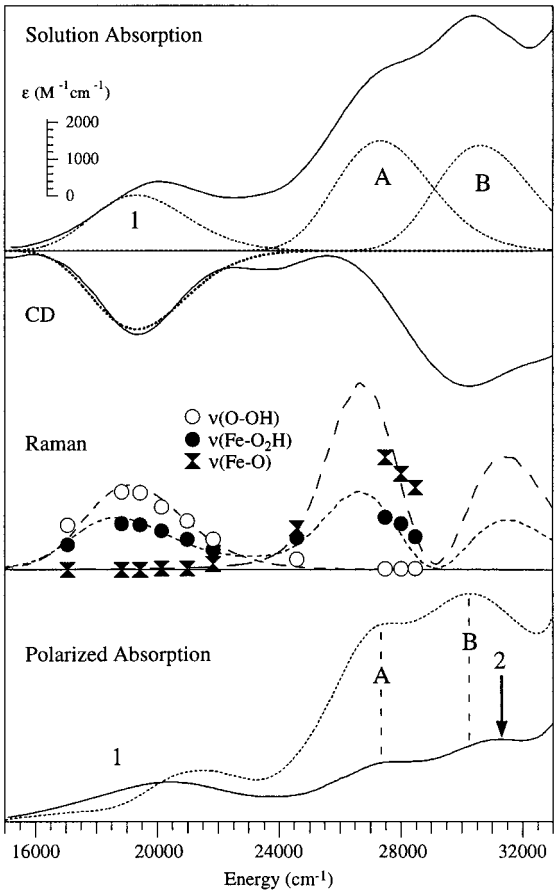

Figure 4. Experimental (300 K) and simulated absorption, CD, and resonance Raman excitation profile data for oxyHr. Top: solution absorption and CD spectra (solid lines, adapted from ref 10) and band shape simulations for transitions 1, A, and B (dotted lines). Center: experimental rR excitation profiles (symbols, adapted from ref 16) and corresponding simulations (broken lines). Bottom: single-crystal absorption spectra for **E** polarized parallel (dotted line) and perpendicular (solid line) to the Fe···Fe vector (adapted from ref 10).

the redox active orbital for efficient superexchange to Fe2 is energetically accessible.

3.2. Oxyhemerythrin. Data Analysis. Published solution absorption and CD spectra,[10] resonance Raman (rR) excitation profiles for the symmetric Fe−O−Fe, the Fe−hydroperoxide, and the O−OH stretching modes[16] (denoted ν(Fe−O), ν(Fe−O_2H), and ν(O−OH), respectively), and polarized single-crystal electronic absorption spectra[10] of oxyHr are shown in Figure 4, and vibrational data for several isotopomers[16,45] are listed in Table 3. Three dominant features denoted 1, A, and B are observed in the absorption spectra. Band 1 peaking at ∼19300 cm^{-1} was previously assigned to a hydroperoxide-to-Fe charge-transfer (CT) transition[10,16,17] because it is primarily **E** ⊥ **c** polarized (i.e., perpendicular to the Fe···Fe vector[14]) and greatly enhances the ν(Fe−O_2H) and ν(O−OH) modes in the rR spectrum. By analogy, band 2 at ∼31000 cm^{-1} that is also **E** ⊥ **c** polarized and not present in the spectra of metHr derivatives[10,46] is assigned to a second hydroperoxide-to-Fe CT transition. Though extensive overlap with other absorption features prevents a detailed analysis, band 2 appears to be weaker than band 1.

Bands A and B are predominantly **E** || **c** polarized and were therefore assigned to oxo-to-Fe CT transitions;[10] however, rR data do not necessarily appear to be consistent with this assignment: (i) both the oxo-related ν(Fe−O) and the hydroperoxide-related ν(Fe−O_2H) modes are resonance enhanced under band A and (ii) the corresponding rR excitation profiles steadily decrease on approaching band B despite the increase in absorption intensity[16] (Figure 4). The peculiar behavior of the UV rR excitation profile for ν(Fe−O) is not unique to oxyHr. From an extensive study of oxo-bridged diferric sites in proteins and model complexes Sanders-Loehr et al.[21] found that the rR excitation profile for ν(Fe−O) generally peaks with fairly minor features in the corresponding absorption spectrum.

In this section, the spectroscopic data in Figure 4 and Table 3 are used to determine the O−O bond strength of the hydroperoxide, to quantitate the hydroperoxide → Fe charge donation, to define the relative strength of the Fe−hydroperoxide π-bonding interaction, and to evaluate and calibrate electronic structure calculations on oxyHr. The major goals of this study are to identify the origin of the unusual spectral features, to explore the nature of the Fe−hydroperoxide and Fe−oxo bonds, and to evaluate the effects of the hydroperoxide and its hydrogen bond to the bridging oxide on the electronic structure and exchange coupling.

Normal Coordinate Analysis. To obtain the eigenvectors of the normal modes associated with the HO_2−Fe−O−Fe unit and to determine the O−O bond strength of the hydroperoxide, a normal coordinate analysis (NCA) was performed on the vibrational data of oxyHr (Table 3). A Urey−Bradly force field was chosen to facilitate comparison with the results obtained for a well-characterized cis μ-1,2 peroxide diferric model complex.[47] To reduce the number of parameters, the HO_2−Fe−O bending mode and the torsional modes were not included in the analysis, and the proton of the hydroperoxide was combined with the terminal O. Further, the HO−O−Fe and Fe−O−Fe bending force constants and the nonbonded interaction constants were assigned fixed values (see Table 3).[48] The force constants of the three remaining internal coordinates, the Fe−O, Fe−O_2H, and O−OH stretches, were fitted to the experimental frequencies (Table 3).

The correspondence between calculated and experimental frequencies for all isotopomers is excellent (Table 3), lending credence to the normal mode descriptions given in Table 4. The potential energy distribution (PED) contributions indicate that ν(O−OH) involves almost pure O−OH stretching motion, whereas the Fe−O_2H and the Fe−O stretches are significantly mixed.[49] The fitted O−O force constant, k(O−O) = 3.3 mdyn/Å, is larger than the value reported for the cis μ-1,2 peroxide Fe(III) dimer,[47] k(O−O) = 3.1 mdyn/Å, where the high O−O stretching frequency of 876 cm^{-1} results from significant mixing between the O−O and Fe−O_2 stretches.[47] Possible sources of the high O−O force constant in oxyHr, including protonation of the peroxide and hydroperoxide → Fe charge donation, will be evaluated below.

Excited-State Analysis. While the rR excitation profiles and polarized single-crystal absorption data in Figure 4 indicate that

(45) Kurtz, D. M., Jr.; Shriver, D. F.; Klotz, I. M. *J. Am. Chem. Soc.* **1976**, *98*, 5033.

(46) Reem, R. C. Thesis, Stanford University, 1986.

(47) Brunold, T. C.; Tamura, N.; Kitajima, N.; Moro-oka, Y.; Solomon, E. I. *J. Am. Chem. Soc.* **1998**, *120*, 5674.

(48) The values used were based on the results of NCAs on the cis μ-1,2 peroxide Fe dimer[47] and oxo-bridged diferric complexes. Changing these values within reasonable limits did not significantly affect the fitted values of the other force constants.

(49) A detailed NCA has been reported for a μ-oxo-bridged diferric model complex. In that dimer ν(Fe−O) is observed at 530 cm^{-1}, and the force constant obtained for the Fe−O stretch is k(Fe−O) = 3.00 mdyn/Å, indicating that the relatively low frequency of ν(Fe−O) in oxyHr reflects a weak Fe−O bond. Czernuszewicz, R. S.; Sheats, J. E.; Spiro, T. G. *J. Am. Chem. Soc.* **1987**, *26*, 2063.

Table 3. Experimental[16,45] and Calculated Vibrational Frequencies for Five Isotopomers of OxyHr[a]

	$^{16}O_2H$		$^{18}O_2H$		$^{16}O^{18}OH$		$^{18}O^{16}OH$		^{18}O(oxo)		
normal mode	obs	calc	obs	calc	obs	calc	obs	calc	obs	calc	force const
ν(O−OH)	844	843	796	796	824	824	817	817		843	k(O−O) = 3.29
ν(Fe−O_2H)	503	504	479	477	503	502	479	478		502	k(Fe−O_2) = 1.91
ν_{as}(Fe−O)	753	754		754		754		754	720	717	
ν(Fe−O)	486	487		492		487		492	472	471	k(Fe−O) = 2.88

[a] Frequencies are in cm^{-1} and stretching force constants k in mdyn/Å (obtained with Fe−O−Fe and Fe−O−OH bending force constants of 0.28 mdynÅ/rad^2 and Fe···Fe and Fe···OH Nonbonded Interaction Constants of 0.08 mdyn/Å). ν(Fe−O) and ν_{as}(Fe−O) are the symmetric and antisymmetric Fe−O−Fe stretching modes, respectively.

Table 4. Normal Mode Descriptions for OxyHr[a]

	eigenvectors (PED)					
normal mode	s(O−OH)	s(Fe−O_2H)	s(Fe−O)	b(Fe−O−OH)	b(Fe−O−Fe)	μ_{eff}[b]
ν(O−OH)	0.35 (94)	−0.11 (6)	0.00 (0)	−0.06 (0)	0.01 (0)	7.4
ν(Fe−O_2H)	0.04 (4)	0.24 (76)	0.05 (11)	−0.18 (6)	−0.10 (2)	9.2
ν_{as}(Fe−O)	0.00 (0)	0.00 (0)	±0.24 (100)	−0.02 (0)	0.00 (0)	8.6
ν(Fe−O)	−0.01 (0)	−0.09 (10)	0.14 (80)	0.10 (2)	−0.17 (6)	11.6

[a] Mass-weighted eigenvectors $\mathbf{L}_n$ and potential energy distribution (PED) contributions (%) in parentheses for the $^{16}O_2H$ isotopomer expressed in terms of a sum of stretching (s) and bending (b) internal coordinates. [b] Effective reduced masses (g/mol), obtained from rediagonalization of the **G** matrix in the normal coordinate space.

Table 5. Excited-State Parameters from a Simultaneous Fit to the Absorption and rR Data of OxyHr (Figure 4)[a]

band	E_0 (cm^{-1})	ϵ (M^{-1} cm^{-1})	Δ(Fe−O_2 H)	Δ(O−OH)	Δ(Fe−O)
1	16550	1760	2.5	−1.8	0.0
A	24600	3490	1.9	0.0	2.9
B	27900	3350	1.9	0.0	2.9

[a] Energies of the zero-phonon transitions, E_0, molar extinction coefficients, ϵ, and dimensionless displacements relative to the ground state, Δ.

band 1 has primarily hydroperoxide-to-Fe CT character, the number of transitions contributing to this feature is uncertain because the absorption and rR profile peaks are shifted relative to each other.[10] Also, the origin of the peculiar behavior of the rR excitation profiles for ν(Fe−O) and ν(Fe−O_2 H) in the region of bands A and B is poorly understood. Therefore, a detailed analysis of the spectroscopic data of oxyHr in Figure 4 was undertaken within the framework of the time-dependent Heller theory.[25] First, the solution absorption and CD spectra were Gaussian fitted to resolve bands 1, A, and B in the absorption spectrum. The corrresponding band shapes were then simultaneously fitted with the rR excitation profiles (a three-mode/three-state problem) to obtain the excited-state parameters listed in Table 5. Simulated absorption and rR excitation profile data are shown in Figure 4.

The correspondence between the experimental and simulated absorption spectra is satisfactory (note that overlap with additional absorption bands complicates an experimental estimate of the intensities of bands A and B), and the experimental rR excitation profiles for all three modes are very well reproduced by the simulation. In the region of band 1, inclusion of more than one band led to considerably poorer fits of the rR profiles, indicating that this feature is due to a single dominant hydroperoxide-to-Fe CT transition. The red shift of the rR excitation profiles relative to the absorption maximum of band 1 is due to the fact that the Raman intensities were quantitated relative to an internal standard,[16] which eliminates their ν^4 dependence, whereas the absorption intensity scales linearly with ν. Remarkably, the simulation also reproduces the experimentally observed decrease in the rR excitation profiles for ν(Fe−O) and ν(Fe−O_2H) above 27000 cm^{-1}, indicating that this behavior is due to interference effects[50] between the oxo-to-Fe CT excited states assigned to bands A and B. By analogy it appears that the peculiar behavior of the UV rR excitation profile for ν(Fe−O) of other oxo-bridged diferric sites[21] also arises from interference effects among oxo-to-Fe CT excited states.

Chart 2. Distortions in the Excited States Corresponding to Bands 1 and A (Figure 4)

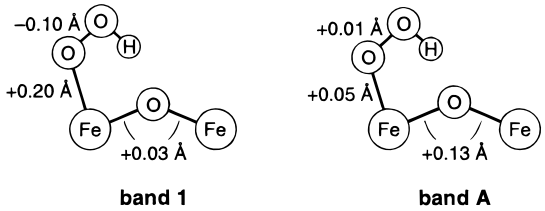

To further characterize the CT excited states corresponding to bands 1 and A, the nuclear distortions of the HO_2−Fe−O−Fe unit were estimated using the following relation between internal coordinate changes, Δr_i (Å), and the fitted dimensionless normal coordinate displacements, Δ_n (Table 5):[34]

$$\Delta r_i = 5.8065 \sum_n L_{i,n}(\Delta_n/\sqrt{\nu_n}) \qquad (3)$$

where $L_{i,n}$ is the ith element of the mass weighted eigenvector, $\mathbf{L}_n$, for the nth normal mode (Table 4). From Chart 2 the major distortions in the hydroperoxide-to-Fe CT excited state (band 1) occur along the Fe−O_2H and O−OH modes. The decrease in the O−OH bond length is consistent with removal of antibonding charge density from the hydroperoxide and demonstrates the CT character of this transition. The nuclear distortions associated with band A indicate that the corresponding excited state has predominantly oxo-to-Fe CT character because the Fe−O_2H bond length increase is insignificant and merely reflects a decrease in effective nuclear charge on iron upon oxo-to-Fe CT excitation. The strong enhancement of ν(Fe−O_2 H) under band A (● in Figure 4) can be attributed to significant out-of-phase coupling between the Fe−O(oxo) and Fe−O_2H stretch motions (Table 4), proposed previously on the basis of qualitative considerations.[22] The normal mode descriptions for the ^{18}O isotopomer (not shown) suggest that this mixing decreases upon $^{16}O \rightarrow {}^{18}O$ isotope exchange of the bridging

(50) Wootton, J. L.; Zink, J. I. *J. Am. Chem. Soc.* **1997**, *119*, 1895.

oxide, consistent with a drop in intensity by 55% of ν(Fe−O_2H) relative to ν(Fe−O) in resonance Raman spectra obtained on μ-^{18}O substituted oxyHr using 27490 cm^{-1} excitation.[22]

In summary, analysis of the spectroscopic data of oxyHr in Figure 4 supports assignments of bands A and B to oxo-to-Fe CT transitions[10,16,21] and suggests that the rR excitation profile for ν(Fe−O) in that region is distorted by interference effects. Further, it permits identification of two hydroperoxide-to-Fe CT bands split by ∼11500 cm^{-1}: a moderatly intense band centered at 19320 cm^{-1} (band 1) and a weaker feature at ∼31000 cm^{-1} (band 2). In the excited state corresponding to band 1 the Fe−O_2H bond length increases by +0.20 Å (Chart 2), indicating that a dominant Fe−hydroperoxide bonding interaction is eliminated upon excitation. Strikingly similar results were obtained for the cis μ-1,2 peroxide ferric dimer[47] where the most intense CT feature associated with the peroxide ligand peaks at 14600 cm^{-1}, separated by ∼11000 cm^{-1} from two closely spaced weaker bands centered around 25500 cm^{-1}. The dominant low-energy transition formally eliminates the Fe−peroxide π-bonding interaction, giving rise to an Fe−peroxide bond length increase by +0.20 Å. By analogy (and supported by the calculations below), band 1 in the spectra of oxyHr (Figure 4) is assigned to a hydroperoxide-to-Fe CT transition that removes the Fe−hydroperoxide π-bonding interaction. The large increase in the Fe−O_2H bond length accompanying this transition (Chart 2, band 1) suggests that the π-contribution to the Fe−hydroperoxide bond is significant because a dominant σ-bonding interaction would greatly reduce distortions along this coordinate.

Hydroperoxide → Fe Charge Donation. The donor strength of a ligand can be estimated from the sum of the integrated absorption intensities of all CT transitions associated with this ligand.[51] While extensive overlap in the region of band 2 prevents a direct quantitation of the total donor strength of the hydroperoxide, the π charge donation from the π^*_π donor orbital into the Fe2 d_π acceptor orbital can be estimated from the intensity of band 1:[51]

$$C_{\pi^*_\pi \rightarrow d_\pi} = \kappa(f/\nu_{max}|\mathbf{r}|^2) \qquad (4)$$

where κ is a constant (9.22 × 10^{-2} Å), f and ν_{max} are the oscillator strength (0.029) and the peak position (19320 cm^{-1}) of band 1, and $|\mathbf{r}|$ is the hydroperoxide−Fe2 bond length (2.00 Å). While the calculated value of $C_{\pi^*_\pi \rightarrow d_\pi}$ is not a quantitative measure of covalency, it permits a correlation with similar complexes;[51] thus, a ratio of 1:1.8 is obtained for the π donor strengths per Fe of the hydroperoxide in oxyHr and the peroxide in the cis μ-1,2 dimer (where f = 0.072, ν_{max} = 14620 cm^{-1}, and $|\mathbf{r}|$ = 1.885 Å[47]). In the corresponding absorption spectra the intensity distributions among the CT transitions associated with these ligands are similar and the excited-state distortions upon $\pi^*_\pi \rightarrow d_\pi$ excitation are virtually identical, suggesting that the relative π contributions to the donor interactions are comparable. Thus, the hydroperoxide → Fe charge donation in oxyHr is ∼3−4 times lower than the total peroxide charge donation to both irons in the cis μ-1,2 dimer. Since electron density is primarily removed from the peroxide π* orbitals that are antibonding with respect to the O−O bond, the stronger O−O bond in oxyHr can be ascribed to protonation of the peroxide.

Electronic Structure Calculations and Comparison to Data. The relevant part of an energy level diagram obtained from a BS calculation on oxyHr is shown in Figure 5 (note that the local coordinate systems on each Fe center (top) have orientations different from those in the deoxyHr structure), and the energies and compositions of the unoccupied Fe d-based MOs are given in Table 6. As for deoxyHr above, the calculated electronic structure description of oxyHr is first evaluated on the basis of experimental data. (i) Using eq 2, a value of J = −214 cm^{-1} is obtained for the exchange coupling constant, roughly a factor of 3 larger than the experimental value[18] of J = −77 cm^{-1} but within the expected error range of density functional calculations.[47,52−54] Significantly, both the experimental and calculated exchange coupling constants for oxyHr are ∼35% smaller in magnitude than the values obtained[47,52,55] for the oxo-bridged diferric complex $[Fe_2O(OAc)_2(tmtacn)_2]^{2+}$ (J_{exp} = −120 cm^{-1} and J_{calc} = −342 cm^{-1} for the corresponding

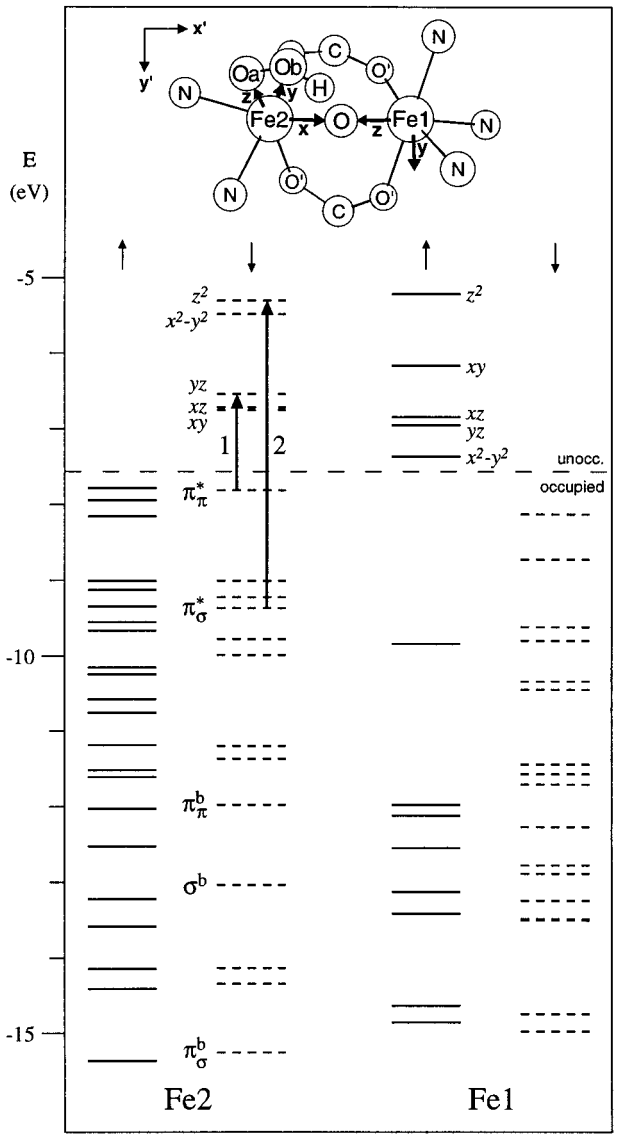

Figure 5. Energy level diagram obtained from a BS (M_S = 0) calculation on oxyHr. Spin-up and spin-down levels are shown by solid and broken lines, respectively. The hydroperoxide-to-Fe CT transitions corresponding to bands 1 and 2 in Figure 4 are indicated by arrows. Top portion: oxyHr model employed, along with the molecular (primed) and local (unprimed) coordinate frames.

(51) Baldwin, M. J.; Root, D. E.; Pate, J. E.; Fujisawa, K.; Kitajima, N.; Solomon, E. I. *J. Am. Chem. Soc.* **1992**, *114*, 10421.

(52) Brown, C. A.; Remar, G. J.; Musselman, R. L.; Solomon, E. I. *Inorg. Chem.* **1995**, *34*, 688.

(53) Zhao, X. G.; Richardson, W. H.; Chen, J.-L.; Li, J.; Noodleman, L.; Tsai, H.-L.; Hendrickson, D. N. *Inorg. Chem.* **1997**, *36*, 1198.

(54) McGrady, J. E.; Stranger, R. *J. Am. Chem. Soc.* **1997**, *119*, 8512.

Table 6. Relative energies, E_{rel} (eV), and Compositions (%) of the Fe d-Based Unoccupied MOs Obtained from a BS Calculation on OxyHr (Figure 5, top)[a]

Spin-Up Orbitals Localized on Fe1

level	E_{rel}	Fe1	O		Fe2	Oa	Ob	
z^2	2.145	71	9	$p_{x'}$	0	0	0	
xy	1.192	79	0		0	0	0	
xz	0.515	52	19	$p_{z'}$	12	6	1	π^*_σ
yz	0.407	74	15	$p_{y'}$	4	1	2	
x^2-y^2	0.000	91	0		1	0	0	
$\sum^b$			43		17	7	3	

Spin-Down Orbitals Localized on Fe2

level	E_{rel}	Fe2	Oa	Ob		O		Fe1
z^2	1.444	67	11	2	π^*_σ	4	$p_{x'}$	2
x^2-y^2	1.263	74	0	0		4	$p_{x'}$	0
yz	0.206	57	25	12	π^*_π	2		0
xz	0.033	79	1	1		9	$p_{z'}$	3
xy	0.000	78	4	2		10	$p_{y'}$	2
$\sum^b$			41	17		29		5

[a] Fe d and O p orbital contributions. Oa (Ob) are the Fe2-bound (terminal) hydroperoxide oxygens, and O denotes the bridging oxide. [b] Sum of the orbital contributions from each ligand and the other Fe ion.

$Fe_2O(O_2CH)_2(NH_3)_6]^{2+}$ model referred to as μ-O,Me_3 tacn below) in which both Fe ions possess ligand environments similar to that of Fe1 in oxyHr. Exchange coupling in these dimers is primarily mediated by the bridging oxide, indicating that the calculated Fe−oxo bonding description for oxyHr is reasonable. (ii) The calculated orbital descriptions (Table 6) can be evaluated on the basis of the electronic absorption spectrum because intensities of CT transitions are primarily governed by the ligand orbital character in the corresponding donor and acceptor MOs.[56] From Table 6 (bottom) two dominant hydroperoxide-to-Fe2 CT bands are expected in the absorption spectrum of oxyHr, as observed (Figure 4), permitting assignment of band 1 to $\pi^*_\pi \rightarrow yz$ (hence, the d_π orbital in eq 4 corresponds to yz) and band 2 to $\pi^*_\sigma \rightarrow z^2$ indicated by arrows in Figure 5 (the π* orbitals are defined in Bonding Description). The corresponding transition energies were calculated using the Slater transition-state method,[57] yielding 10920 and 29790 cm^{-1}, respectively. While the value obtained for the $\pi^*_\sigma \rightarrow z^2$ transition compares reasonably well with the peak position of band 2 ($\sim$31000 cm^{-1}), the calculated energy for the $\pi^*_\pi \rightarrow yz$ transition is 43% lower than the maximum of band 1 (19320 cm^{-1}). Thus, the calculated splitting between the π^*_π and yz orbitals (see Bonding Description) is too small, and the π donor strength of the hydroperoxide in oxyHr is overestimated by the calculation: the computed π^*_π contributions to the Fe2 yz-based MOs in oxyHr (Table 6) and the cis μ-1,2 dimer[47] are comparable, yet the experimental ratio is 1:1.8 (*vide supra*). In summary, the calculated bonding description of oxyHr is fairly reasonable although the hydroperoxide → Fe2 π-donor interaction is overestimated by $\sim$45%.

Bonding Description. Nature of the Fe d-Based Orbitals. In the BS ground state, the five unpaired electrons on each iron occupy Fe d-based "majority-spin" MOs, leading to a large exchange stabilization of these orbitals relative to their unoccupied "minority-spin" counterparts and, consequently, to significant mixing with ligand orbitals. In the following analysis the dominant metal−ligand bonding interactions are therefore inferred from the compositions of the unoccupied minority-spin MOs that reflect the primarily metal-centered excess (i.e., uncompensated) majority-spin density.

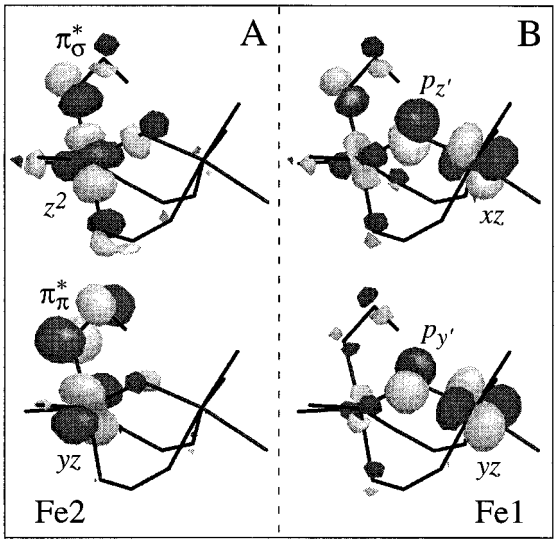

Figure 6. Boundary surface plots of the relevant iron d-based unoccupied orbitals localized on Fe2 (A, spin-down MOs) and Fe1 (B, spin-up MOs), obtained from a BS ($M_S = 0$) calculation on oxyHr.

The splitting pattern of the Fe1 d-based unoccupied spin-up MOs (Figure 5, right) is characteristic of Fe(III) in bent oxo-bridged dimers:[47,52] the z^2 orbital is involved in a σ-antibonding interaction with the oxo $p_{x'}$ orbital, and the xz and yz orbitals exhibit strong π-antibonding interactions with the oxo $p_{z'}$ and $p_{y'}$ orbitals, respectively (Figure 6B). In contrast, the splitting pattern of the Fe2 d-based unoccupied spin-down MOs (Figure 5, left) reflects a fairly octahedral LF environment. The σ-antibonding interaction with the hydroperoxide π^*_σ orbital located in the O_2H plane is sufficiently strong to reorient the z^2 orbital toward the Fe2−O_2H bond vector (Figure 6A, top). The yz orbital is involved in a strong π-antibonding interaction with the second hydroperoxide π* orbital, designated π^*_π (Figure 6A, bottom), and the xz and x^2-y^2 orbitals exhibit strong π-antibonding interactions with the oxo $p_{z'}$ and $p_{y'}$ orbitals, respectively (Table 6). As a result the t_{2g} orbital splitting of Fe2 is unusually small for Fe(III) in an oxo-bridged dimer[52] (cf. Figure 5, left (Fe2) *vs* right (Fe1)).

The large difference in calculated electronic structures for Fe1 and Fe2 is compatible with Mössbauer data. Typically, the strong axial LF component associated with the bridging oxide in oxo-bridged diferric sites gives rise to a large quadrupole splitting, $\Delta E_Q = 1.5-2.0$ mm/s.[24] In oxyHr the quadrupole splitting of one iron is also large, $\Delta E_Q \approx 2.0$ mm/s,[23] whereas the second iron exhibits an unusually small ΔE_Q value of $\sim$1.0 mm/s,[23] consistent with less distorted electronic surroundings of that iron. Thus, although a direct experimental link between the Mössbauer parameters and the Fe centers in oxyHr has yet to be established, it appears reasonable to assign the smaller quadrupole splitting in oxyHr to Fe2.

Nature of the Fe2−Hydroperoxide Bond and the Effects of the Proton. The Fe2−hydroperoxide bonding interactions can be inferred from the Fe2 d-based unoccupied spin-down MOs (Figure 6A) as these orbitals correspond to the metal−ligand antibonding counterparts of the ligand-based bonding MOs. Thus, the dominant σ- and π -bonding interactions involve

(55) Hartman, J. R.; Rardin, R. L.; Chaudhuri, P.; Pohl, K.; Wieghardt, K.; Nuber, B.; Weiss, J.; Papaefthymiou, G. C.; Frankel, R. B.; Lippard, S. J. *J. Am. Chem. Soc.* **1987**, *109*, 7387.

(56) (a) Ros, P.; Schuit, G. C. A. *Theor. Chim. Acta (Berlin)* **1966**, *4*, 1. (b) Van der Avoird, A.; Ros, P. *Theor. Chim. Acta (Berlin)* **1966**, *4*, 13.

(57) Slater, J. C. *The Calculation of Molecular Orbitals*; John Wiley & Sons: New York, 1979.

the z^2/π_σ^* and yz/π_π^* orbitals, respectively. From Table 6, the contributions from the hydroperoxide π_π^* (even scaled by 45%, *vide supra*) and π_σ^* orbitals to the Fe2 d-based MOs are ~40% larger than the oxo p orbital contributions. Though this result does not necessarily imply that the Fe2−hydroperoxide bonding interaction is dominant (i.e., the stabilization energy and the mixing coefficients scale linear and quadratic, respectively, with the energy separation between interacting orbitals), it suggests that the hydroperoxide is at least an equally strong donor as the bridging oxide.

In comparison with the peroxide in the cis μ-1,2 dimer, however, the donor strength of the hydroperoxide in oxyHr is lower (*vide supra*). Nevertheless, the O−O force constant is higher in the protein, consistent with a recent study of a μ-1,1 hydroperoxide Cu(II) dimer.[58] Protonation was found to increase the electrophilicity of the peroxide, thereby decreasing the charge donation to the metal by ~40%. The proton stabilizes the orbitals on the oxygen to which it is bound (cf. the small orbital contributions from Ob relative to Oa in the Fe2 d-based unoccupied MOs of oxyHr, Table 6), and both the intraperoxide π-bonding and π-antibonding interactions are disrupted by protonation, the net result being an increase in O−O bond strength.[58]

Effects of the Hydrogen Bond. In this section the effects of the hydrogen bond in oxyHr between the hydroperoxide and the bridging oxide, believed to be responsible for the reduced ground-state exchange coupling and the low frequency of ν(Fe−O) relative to other oxo-bridged diferric complexes, are explored through density functional calculations by correlating between the experimentally calibrated electronic structure descriptions of oxyHr and μ-O,Me$_3$tacn. The models used for this correlation include (top of Figure 7) oxyHr, μ-O,Me$_3$tacn, and μ-O,O$_2$H^{rot}, the latter having the peroxide rotated so as to eliminate the hydrogen bond with the bridging oxide[59] (energy level diagrams for μ-O,O$_2$H^{rot} and μ-O,Me$_3$tacn are shown in Figures S1 and S2, respectively, Supporting Information). From the difference in calculated total energies for oxyHr and μ-O,O$_2$H^{rot}, a value of 5.5 kcal/mol is obtained for the hydrogen bond energy in oxyHr. This value is reasonable in magnitude and consistent with Raman data that reveal the presence of a strong hydrogen bond in oxyHr.[22] The relevant part of a qualitative MO diagram defining this hydrogen bond interaction is presented in Figure S3, and boundary surface plots of the key orbitals are shown in Figure S4.

The effectiveness of the Fe d-based MOs in mediating antiferromagnetic coupling is governed by the extent of orbital contributions from the bridging oxide and the second iron (Figure 7, Table 7). Thus, the dominant Fe1-derived superexchange pathways in oxyHr involve the *xz*- and *yz*-based spin-up MOs that are π-antibonding to the bridging oxide (Figure 6B). Since these orbitals are unoccupied, their Fe2 character relates to the extent of hole delocalization from Fe1 onto Fe2 and, therefore, to the extent of electron delocalization from Fe2 onto Fe1. The total oxo and Fe2 orbital contributions to the Fe1 d-based MOs in oxyHr, μ-O,O$_2$H^{rot}, and μ-O,Me$_3$tacn are comparable, suggesting that the extent of Fe1 → Fe2 electron delocalization in oxyHr is only slightly affected by the hydrogen bond between the hydroperoxide and the bridging oxide.[60]

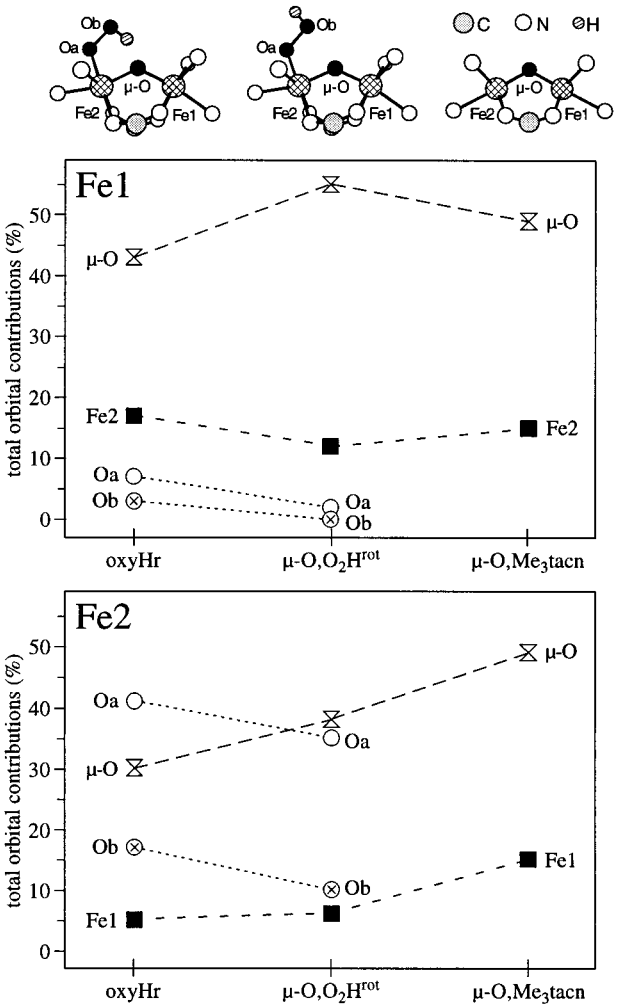

Figure 7. Total O p- and Fe d-orbital contributions from the hydroperoxide (Oa, Ob), the bridging oxide (μ-O), and the adjacent iron to the Fe1 and Fe2 d-based unoccupied MOs for the three structures shown on the top.

The dominant superexchange pathways in oxyHr involving the Fe2-based MOs are similar in nature to the Fe1-derived pathways, but the lower orbital contributions from the oxo and the second iron indicate that their effectiveness is greatly reduced (Figure 7, Table 7). Elimination of the hydrogen bond in μ-O,O$_2$H^{rot} increases the total oxo → Fe charge donation at the expense of the hydroperoxide → Fe1 charge donation because the proton is no longer shared with the bridging oxide. The increase in Fe1 orbital contributions to the Fe2 d-based MOs is insignificant, however, corresponding to the small change in J_{calc} (Table 7). Alternatively, replacement of the hydroperoxide ligand on Fe2 by NH$_3$ (a weaker donor) in μ-O,Me$_3$tacn results in a significant increase in oxo and Fe1 orbital contributions to the Fe2 d-based unoccupied MOs (Figure 7) and, consequently, in a substantially larger $|J_{calc}|$ value (Table 7). Thus, the weak exchange coupling in oxyHr relative to μ-O,Me$_3$tacn appears to be due primarily to the presence of two strong donors (i.e., the hydroperoxide and the bridging oxide) bound to Fe2 that lower the effective nuclear charge on that iron and reduce Fe1 → Fe2 electron delocalization.

Along the series of dimers in Figure 7, the total oxo → Fe charge donation summed over both metal ions increases by 27% from oxyHr to μ-O,O$_2$H^{rot}, but only 5% from μ-O,O$_2$H^{rot} to

(58) Root, D. E.; Mahroof-Tahir, M.; Karlin, K. D.; Solomon, E. I. *Inorg. Chem.* **1998**, *37*, 4838.

(59) The coordinates of the Oa, Ob, μ-O, and H atoms were reoptimized with the remainder of the model kept frozen.

(60) An experimental verification of the minor effect of the hydrogen bond upon one Fe−oxo bonding interaction in oxyHr is provided by Mössbauer data. From studies of hydroxo-bridged diiron(III) models, the quadrupole splitting of Fe centers possessing ligand environments similar to that of Fe1 is small, $\Delta E_Q = 0.3-0.7$ mm/s.[24] The quadrupole splitting of one iron in oxyHr ($\Delta E_Q \approx 2.0$ mm/s),[23] however, is even among the largest observed values for Fe(III) in oxo-bridged dimers.[24]

Table 7. Compositions (%) of the Fe d-Based Unoccupied MOs Obtained from BS Calculations on the Three Complexes in Figure 7 (top)[a]

Spin-Up Orbitals Localized on Fe1

oxyHr						μ-O,O_2H^{rot}						μ-O,Me_3tacn			
level	Fe1	O	Fe2	Oa	Ob	level	Fe1	O	Fe2	Oa	Ob	level	Fe1	O	Fe2
z^2	71	9	0	0	0	z^2	68	11	0	0	0	z^2	67	11	0
xy	79	0	0	0	0	xy	79	0	0	0	0	xy	72	0	0
xz	52	19	12	6	1	xz	52	24	10	2	0	xz	53	22	14
yz	74	15	4	1	2	yz	75	20	1	0	0	yz	79	16	1
x^2-y^2	91	0	1	0	0	x^2-y^2	91	0	1	0	0	x^2-y^2	90	0	0
$\sum^b$		43	17	7	3			55	12	2	0			49	

Spin-Down Orbitals Localized on Fe2

oxyHr						μ-O,O_2H^{rot}						μ-O,Me_3tacn			
level	Fe2	Oa	Ob	O	Fe1	level	Fe2	Oa	Ob	O	Fe1	level	Fe2	O	Fe1
z^2	67	11	2	5	0	z^2	65	9	1	8	0	z^2	67	11	0
x^2-y^2	74	0	0	4	0	x^2-y^2	75	2	0	2	0	xy	72	0	0
yz	57	25	12	2	0	xz	67	20	6	2	0	xz	53	22	14
xz	79	1	1	9	3	xz	70	0	1	15	5	yz	79	16	1
xy	78	4	2	10	2	xy	79	4	2	11	1	x^2-y^2	90	0	0
$\sum^b$		41	17	30	5			35	10	38	6			49	15
ν(Fe−O)[c]					486						na				540
J_{calc}[d]					−214						−232				−342
J_{exp}[d]					−77						na				−120

[a] Fe d and O p orbital contributions. Oa (Ob) are the Fe2-bound (terminal) hydroperoxide oxygens, and O denotes the bridging oxide. [b] Sum of the orbital contributions from each ligand and the other Fe ion. [c] Experimental frequencies of the symmetric Fe−O−Fe stretching mode[16,52] in cm^{-1} (na: not available). [d] Calculated and experimental[18,55] exchange coupling constants in cm^{-1}.

μ-O,Me_3tacn because the weaker Fe2−O bonding interaction in μ-O,O_2H^{rot} is largely compensated by the stronger Fe1−O bond. From a NCA on the Fe−O−Fe unit, reducing one Fe−O force constant while increasing the other has little effect on ν(Fe−O), suggesting that elimination of the hydrogen bond in oxyHr would raise the frequency of ν(Fe−O). This model is supported by experimental data for hydroxy-metHr where a mixture of two distinct conformers exists.[22] For the hydrogen-bonded cis conformer, ν(Fe−O) peaks at 492 cm^{-1}, shifting to 506 cm^{-1} upon elimination of the hydrogen bond in the trans conformer.

In summary, the BS calculations on the three models in Figure 7 suggest that the relatively weak exchange coupling in oxyHr is due primarily to the strong donor interaction of the hydroperoxide with Fe2 that localizes this center and reduces the Fe1 → Fe2 electron delocalization. The fairly strong hydrogen bond between the hydroperoxide and the bridging oxide appears to be of minor importance with respect to the reduced exchange coupling; however, it produces a substantial reduction in the total oxo → Fe charge donation which is reflected in the small Fe−O force constant (Table 4).

4. Discussion

Over the past 40 years the two physiologically relevant forms of hemerythrin (Hr), deoxyHr and oxyHr, have been spectroscopically and crystallographically well characterized.[4] Their interconversion, involving an electron transfer (ET) from each Fe(II) of deoxyHr to O_2 binding at a single metal center coupled with a proton transfer (PT) to yield the oxo-bridged oxyHr site with a terminal hydroperoxide (Chart 1), however, is rather poorly understood. In an effort toward obtaining molecular level insight into this fascinating reaction mechanism, we have investigated the electronic structures of the reduced and oxidized sites of Hr. Advantage has been taken of the large body of spectroscopic data that exist for deoxyHr and oxyHr, which has permitted evaluation and calibration of density functional calculations on simplified models of these sites. The key features of the electronic structures of deoxyHr and oxyHr are summarized below, and their relation to reversible dioxygen binding is discussed.

Analysis of the magnetic susceptibility data of deoxyHr (Figure 1) indicates that the two ferrous ions of the active site are weakly antiferromagnetically coupled, $J = -14(2)$ cm^{-1}, in good agreement with earlier results.[9,15] This value is consistent with the presence of a hydroxo bridge at the deoxyHr site[9,14] and implies that at 300 K the entire manifold of ground-state spin sublevels is thermally populated (i.e., the entire exchange splitting is 280 cm^{-1}) and can thus participate in the reaction with O_2. The redox active orbital containing the extra electron of the five-coordinate iron (Fe2) is properly oriented for a π-bonding interaction with one of the half-occupied π^* orbitals of dioxygen approaching along the open coordination site (Figure 3). The redox active orbital on the six-coordinate iron (Fe1) is oriented perpendicular to the Fe1−hydroxide bond; however, its separation from the lowest unoccupied orbital that is π-antibonding to the hydroxide is very small, and reorientation of the redox active orbital on Fe1 for electron transfer to O_2 through superexchange with Fe2 is energetically accessible.

The μ-oxo diiron(III) structural motif has been under intense study because of its occurrence in several metalloprotein active sites.[19] Several unique spectral features of oxyHr have been poorly understood, however. Analysis of the resonance Raman excitation profile for the symmetric Fe−O−Fe stretching mode ν(Fe−O) using the time-dependent Heller theory[25,33] leads to the proposal that the peculiar behavior in the UV region to peak with fairly minor absorption features[16] (Figure 4) can be attributed to interference effects[50] between the oxo-to-Fe charge-transfer (CT) excited states corresponding to bands A and B.

(61) The substantial reduction in the total oxo → Fe charge donation because of the hydrogen bond in oxyHr (Figure 7) might be expected to perturb the oxo-to-Fe CT absorption spectrum, yet other oxo-bridged diferric sites exhibit fairly similar absorption spectra in that region. According to the valence bond configuration interaction (VBCI) model,[52,62] the low energy of the oxo-to-Fe CT transitions in these dimers contributing to the absorption spectrum below 40000 cm^{-1} arises from large antiferromagnetic coupling in the corresponding excited states and involves oxo p orbitals that are oriented perpendicular to the hydrogen bond in oxyHr and thus should not be strongly affected by this interaction.

The low frequency of ν(Fe−O) in oxyHr[16] (Table 3) reflects the fairly strong hydrogen bond between the hydroperoxide and the bridging oxide (Figure S4) that produces a substantial reduction in the total oxo → Fe charge donation (Figure 7).[61,62] The contribution from this hydrogen bond to the unusually small exchange coupling constant $J = -77$ cm^{-1} in oxyHr[18,20] seems minor, however, contrasting previous proposals. Rather, the weak exchange coupling appears to be due to the strong donor interaction of the hydroperoxide with Fe2 that localizes this center and reduces Fe1 → Fe2 electron delocalization (Figure 7, bottom). Alternatively, electron delocalization from Fe2 onto Fe1 through the mixed σ/π pathway (Figure 6B, top) is substantial. Significantly, this superexchange pathway involves an Fe1-centered unoccupied orbital that is π rather than σ-antibonding to the bridging oxide and thus may serve as an ET pathway between Fe2 and a *low-lying* orbital on Fe1.

The calculated electronic structure of Fe1 in oxyHr (Figures 5 (right) and 6B) indicates that the ligand field (LF) felt by this iron is dominated by the bridging oxide, which is typical for Fe(III) in oxo-bridged dimers.[52] In contrast, the bonding interactions of Fe2 with two strong donor ligands (the hydroperoxide and the bridging oxide) give rise to net fairly symmetrical electronic surroundings for that iron (minor t_{2g} orbital splitting, Figure 5 (left)). The large differences in calculated electronic structures for the two Fe centers are consistent with Mössbauer data and strongly suggest that the quadrupole splittings of $\Delta E_Q \approx 2.0$ and 1.0 mm/s[23] are associated with Fe1 and Fe2, respectively.

Charge donation from the hydroperoxide mainly involves the π^*_π orbital that is π-bonding to the Fe2 *yz* orbital, the latter having a similar orientation to the Fe2-based redox active orbital in deoxyHr (cf. Figures 3 and 6). In comparison with the bridging peroxide in a well-characterized cis μ-1,2 diferric complex,[47] the hydroperoxide in oxyHr is a weaker donor. Though electron density is primarily removed from the peroxide π^* orbitals that are antibonding with respect to the O−O bond, this bond is stronger in oxyHr. Similar results were obtained by Root et al.[58] from an electronic structure study of a μ-1,1 hydroperoxide Cu(II) dimer and its deprotonated analogue, suggesting that a strong O−O bond and low peroxide donor strength are general features of hydroperoxide−metal complexes.

In principle, protonation can activate the peroxide for further reduction.[58] However, the presence of a μ-O diiron(III) core at the oxyHr site stabilizes the diferric oxidation state, and the associated large antiferromagnetic exchange coupling between the Fe(III) centers significantly lowers the energy of the singlet ground state.[63] Two-electron reduction of the hydroperoxide in oxyHr would result in the formation of a μ-O diiron(IV) site. In isoelectronic μ-O dimanganese(III) complexes, exchange coupling is very weak[64] because the Mn z^2-based orbital pointing toward the bridging oxide is unoccupied (cf. the dominant superexchange pathway in oxyHr, Figure 6B, top). Thus, two-electron oxidation of the μ-O diiron(III) core to generate an oxo-bridged diiron(IV) species would have to overcome a significant energy barrier associated with the reduction in the singlet ground-state stabilization due to a large decrease in antiferromagnetic exchange coupling.

Acknowledgments. We thank Drs. Sabine Pulver and Cecelia Campochiaro for collecting the SQUID magnetic susceptibility data on deoxyHr and Dr. Frank Neese for his help with the zero-field splitting analysis. Financial support by the NSF-Biophysics Program Grant MCB 9816051 is gratefully acknowledged.

Supporting Information Available: Energy level diagrams from BS calculations on μ-O,O$_2$H^{rot} and μ-O,Me$_3$tacn, MO diagram defining the hydrogen bond interaction in oxyHr boundary surface plots of the corresponding key orbitals, and tables reporting the coordinates of all the models used for the calculations (PDF). This material is available free of charge via the Internet at http://pubs.acs.org.

JA990334S

(62) Tuczek, F.; Solomon, E. I. *Inorg. Chem.* **1993**, *32*, 2850.

(63) In the VBCI formalism[62] exchange coupling arises from a *net* stabilization of the singlet ground state through second-order configuration interaction with metal-to-metal and double CT excited states.

(64) Wieghardt, K. *Angew. Chem., Int. Ed. Engl.* **1989**, *28*, 1153.